Integral sliding mode impedance control based on exponential reaching law for grinding robot

Lin Jia[1], Huan Chen[1], Changfan Zhang[1], Zhongmei Wang[1] , and Li Liu[2]

[1] College of Railway Transportation, Hunan University of Technology, Zhuzhou, Hunan 412000, China
[2] College of Engineering and Design, Hunan Normal University, Changsha, Hunan 410081, China
Corresponding author, E-mail: wangzhongmei@hut.edu.cn

Abstract. An improved impedance control method for grinding robots to enhance the machining quality of free-form workpieces is proposed. This method combines integral sliding mode control with the exponential reaching law to improve the design of impedance control algorithms. Firstly, by leveraging the system's impedance parameter model and contact impedance force, the robot's ideal impedance trajectory is calculated. Subsequently, an integral sliding mode impedance control method, utilizing the exponential reaching law, is developed to accurately follow the impedance trajectory. The adoption of the reaching rate can mitigate the chattering issue that occurs in sliding mode control. Finally, the stability of the system is validated using Lyapunov theory, followed by simulations and experiments. Simulation and experimental results demonstrate that the proposed method offers superior dynamic and static performance.

Keywords: grinding robot; impedance control; integral sliding mode; exponential reaching law.

1 Introduction

Grinding is a pivotal processing stage in the intricate production cycle of castings. However, traditional manual grinding methods often suffer from inefficiency and reduced accuracy, in addition to the widespread issues of excessive noise and dust that pose risks to operator health. The use of robots can improve the consistency of grinding work and significantly improve the working conditions for frontline workers [1]. Today, the extensive use of robotic grinding in industries such as aerospace, shipbuilding, and automotive manufacturing highlights its transformative potential.

The interaction between the grinding tip and the workpiece significantly impacts the robot control system's performance and, consequently, the quality of the grinding operation. Therefore, this interaction is a crucial consideration in the design of the grinding robot controller. Typical interaction control techniques encompass impedance control and hybrid force/position control. Impedance control demonstrates excellent force control performance, making it widely used in grinding robots. As an illustration,

in [2], a method for automatically adjusting robot grinding behavior using an impedance model is proposed to address the issues of high labor intensity, inconsistent quality, and poor safety and hygiene in manual sanding operations, thereby enabling robots to operate on uncertain objects with minimal human involvement. In [3], a nonlinear impedance control method is introduced for collaborative robot grinding, which successfully enhances the stability of the robot grinding force. The authors of [4] propose an adaptive variable impedance control algorithm to tackle the constant force control issue in flexible grinding processes, achieving the objectives of adjusting system impedance and reducing force tracking deviation.

The sliding mode control method exhibits excellent robustness and can be used to enhance the impedance control performance of robots. Many researchers are investigating the integration of sliding mode and impedance control for various robotic applications. In [5], a method combining a linear sliding mode with multiple degrees of freedom and impedance control is proposed for distributing contact force between a single slave robotic arm and several master robotic arms, achieving the goals of maintaining MTS stability and obtaining high-precision motion. In [6], a method integrating sliding mode and impedance control is presented to address full contact interference in interferometric autonomous underwater vehicles (I-AUVs), successfully achieving precise position and force tracking. The authors of [7] propose a method that combines sliding mode and impedance control for fully actuated unmanned aerial vehicles performing contact-based aerial manipulation tasks, aiming to reduce chattering and construct a robust fault-tolerant motion/force controller. The study in [8] introduces a method combining sliding mode, impedance control, and fuzzy adaptive switching gain for the impedance control of fracture reduction robots, enhancing system robustness. [9] presents an integral fuzzy sliding mode impedance control strategy combined with time delay estimation for robot-assisted cooperative rehabilitation training problems, aiming to suppress impedance errors and eliminate dynamic model nonlinearity and interference. In this process, the integral sliding surface, due to the presence of an integral element, smooths the dynamic response of the system and effectively suppresses chattering.

Furthermore, incorporating a reaching law into the design of sliding mode controllers can streamline the design process and significantly enhance the dynamic performance of the control system[10-12]. For instance, in [13], a method based on the reaching law of difference equations with minimum values is applied to discrete-time sliding mode control problems, suppressing chattering and limiting the rate of change of sliding variables. In [14], an advanced approach law sliding mode control strategy is presented for the speed control problem of permanent magnet synchronous motors, accelerating convergence speed and reducing chattering. In [15], an enhanced torque sharing function control method for switched reluctance motors is proposed, utilizing sliding mode control with a novel sliding mode reaching law to suppress torque ripple and increase approaching speed.

Based on the above research, we conducted research on impedance control algorithms for grinding robots based on exponential reaching law and integral sliding mode surface(ERL-ISMIC). The remainder of this paper is structured as follows: Section 2 introduces the impedance dynamic model for a grinding robot. Section 3 details the integral sliding mode impedance control algorithm based on the exponential reaching

law. Section 4 presents the simulation results to verify the effectiveness and performance of the proposed method. Section 5 further validates the effectiveness of the integral sliding mode impedance control method based on the exponential reaching law through experimental testing. Section 6 offers the conclusions.

2 Impedance control model for grinding robots

To analyze the contact characteristics of the robot end effector, a dynamic equation needs to be constructed in the task coordinates using the end effector's position as a variable, based on the traditional dynamic model that uses joint positions as variables. Considering external disturbances and modeling uncertainties, a typical robot dynamic model using joint angles as variables is as follows[16]:

$$D(q)\ddot{q} + C(q,\dot{q}) + G(q) + \Delta(q,\dot{q},\ddot{q}) = \tau \tag{1}$$

where $q,\dot{q},\ddot{q} \in R^{n\times 1}$ are the vectors of joint position, velocity, and acceleration, respectively; $D(q) \in R^{n\times n}$ is the symmetric positive definite inertia matrix; $C(q,\dot{q}) \in R^{n\times n}$ is the Coriolis force and centrifugal force vector; $G(q) \in R^{n\times 1}$ expresses the nominal gravity vector; $\tau \in R^{n}$ is the joint torque input vector; and $\Delta(q,\dot{q},\ddot{q})$ is the disturbance , $\Delta(q,\dot{q},\ddot{q}) = \Delta D(q)\ddot{q} + \Delta C(q,\dot{q})\dot{q} + \Delta G(q) + \tau_d$.

Impedance control aims to regulate the contact force between the grinding robot's end effector and the workpiece by controlling its position within the Cartesian coordinate system. Therefore, it is essential to transform the dynamic equation from one that uses joint angles as variables to one that employs the end effector position in the Cartesian coordinate system as the variable. If l is the end position vector of the robot, which is a function of the joint angles, then the joint angles and the end position satisfy the following relationship[17]:

$$\begin{aligned} l &= h(q) \\ \dot{l} &= J(q)\dot{q} \end{aligned} \tag{2}$$

where $J(q)$ is the Jacobian matrix of the robot.

Assuming the contact force between the end effector of the grinding robot and the workpiece is F_{re} , the dynamics of the target impedance is[18]:

$$M(\ddot{l}_c - \ddot{l}) + B(\dot{l}_c - \dot{l}) + K(l_c - l) = F_{re} \tag{3}$$

where l_c is the ideal end trajectory and l is the actual end trajectory, and when there is a deviation between the two, relevant forces will be generated; M is the mass coefficient matrix; B is the damping coefficient matrix; and K is the stiffness coefficient matrix.

The dynamic model based on the end position can be established as follows[19]:

$$D_l(q)\ddot{l} + C_l(q,\dot{q})\dot{l} + G_l(q) + F_{re} + \Delta_l(q,\dot{q},\ddot{q}) = F_l \tag{4}$$

where:

$D_l(q) = J^{-T}(q)D(q)J^{-1}(q)$,

$C_l(q) = J^{-T}(q)(C(q,\dot{q}) - D(q)J^{-1}(q)\dot{J}(q))J^{-1}(q)$,

$G_l(q) = J^{-T}(q)G(q)$,

$\Delta_l(q,\dot{q},\ddot{q}) = J^{-T}(q)\Delta(q,\dot{q},\ddot{q})$.

In the actual grinding process, the expected end trajectory l_c may be unreachable, so it is necessary to obtain the ideal impedance trajectory l_d through an impedance model. The impedance model is as follows[20]:

$$M\ddot{l}_d + B\dot{l}_d + Kl_d = -F_{re} + M\ddot{l}_c + B\dot{l}_c + Kl_c \tag{5}$$

3 Integral Sliding Mode Impedance Control Algorithm

We define the state variable of the end position error of the grinding robot in the Cartesian coordinate system as[21]:

$$e = l_d - l \tag{6}$$

Then, one has

$$\begin{aligned} \ddot{e} &= \ddot{l}_d - \ddot{l} \\ &= \ddot{l}_d - D_l^{-1}(F_l - C_l\dot{l} - G_l - F_{re} - \Delta_l) \end{aligned} \tag{7}$$

We define the integral sliding mode surface as[22] :

$$s = c_1 e + \dot{e} + c_2 \int e \tag{8}$$

where $s = [s_1; s_2; ...; s_n]$, and c_1 and c_2 are constants greater than zero.

Then there are:

$$\begin{aligned} \dot{s} &= c_1\dot{e} + \ddot{e} + c_2 e \\ &= c_1\dot{e} + \ddot{l}_d - D_l^{-1}(F_l - C_l\dot{l} - G_l - F_{re} - \Delta_l) + c_2 e \end{aligned} \tag{9}$$

Then we select the law of exponential reaching[23]:

$$\dot{s} = -\varepsilon\,\mathrm{sgn}(s) - ks \tag{10}$$

where ε and k are positive real constants.

The design control law is:

$$F_l = D_l(c_1\dot{e} + \ddot{l}_d + c_2 e + \varepsilon \operatorname{sgn}(s) + ks) + C_l\dot{l} + G_l + F_{re} + D_l \operatorname{sgn}(s)\left\|D_l^{-1}\right\|\hat{\Delta} \quad (11)$$

where $\hat{\Delta} \geq \|\Delta\|$.

The stability proof is as follows:

The Lyapunov function is defined as follows[24] :

$$V = \frac{1}{2}s^T s \quad (12)$$

Then we derive it and substitute Equation (9) to obtain

$$\dot{V} = s^T\dot{s} = s^T(c_1\dot{e} + \ddot{l}_d - D_l^{-1}(F_l - C_l\dot{x} - G_l - F_{re} - \Delta_l) + c_2 e) \quad (13)$$

Substituting control law Equation (11) into Equation (13) yields

$$\begin{aligned}
\dot{V} &= s^T(-\varepsilon \operatorname{sgn}(s) - ks - D_l^{-1}(D_l \operatorname{sgn}(s)\left\|D_l^{-1}\right\|\hat{\Delta} - \Delta)) \\
&= -\varepsilon\|s\| - k\|s\|^2 - s^T D_l^{-1}(D_l \operatorname{sgn}(s)\left\|D_l^{-1}\right\|\hat{\Delta} - \Delta) \\
&= -\varepsilon\|s\| - k\|s\|^2 + s^T D_l^{-1}\Delta - \|s\|\left\|D_l^{-1}\right\|\hat{\Delta} \\
&\leq -\varepsilon\|s\| - k\|s\|^2 + \left\|s^T\right\|\left\|D_l^{-1}\right\|\|\Delta\| - \|s\|\left\|D_l^{-1}\right\|\hat{\Delta} \\
&= -\varepsilon\|s\| - k\|s\|^2 + \|s\|\left\|D_l^{-1}\right\|\|\Delta\| - \|s\|\left\|D_l^{-1}\right\|\hat{\Delta} \\
&= -\varepsilon\|s\| - k\|s\|^2 + \|s\|\left\|D_l^{-1}\right\|(\|\Delta\| - \hat{\Delta})
\end{aligned}$$

Since both ε and k are positive numbers and $\hat{\Delta} \geq \|\Delta\|$, then $\dot{V} \leq 0$. If and only if $s(t) = 0$, $\dot{V}(t) = 0$. When $\dot{V} \equiv 0$, $s \equiv 0$. According to the LaSalle invariant set principle[25], when $t \to \infty$, $s \to 0$, $e \to 0$, the closed-loop control system is asymptotically stable. Meanwhile, by adjusting the appropriate values of ε and k, the speed of the system approaching the sliding surface can be increased and the speed of motion in sliding mode can be reduced, thereby achieving the goal of improved chattering.

4 Simulation analysis

To demonstrate the effectiveness of the proposed method, we use the grinding robot as the control object, simplify it into a two-joint model based on the assumptions stated in the paper, and conduct simulation verification on the Matlab R2022b platform.

Considering friction and external disturbances, the dynamic equation of the grinding robot in the Cartesian coordinate system is shown in Equation (4):

$$D_l(q)\ddot{l} + C_l(q,\dot{q})\dot{l} + G_l(q) + F_{re} + \Delta_l(q,\dot{q},\ddot{q}) = F_l$$

The system parameters of the robot used in the simulation are

$$D(q)=\begin{bmatrix} D_{11}(q_2) & D_{12}(q_2) \\ D_{21}(q_2) & D_{22}(q_2) \end{bmatrix}, C(q,\dot{q})=\begin{bmatrix} C_{11}(q_2) & C_{12}(q_2) \\ C_{21}(q_2) & C_{22}(q_2) \end{bmatrix}, G(q)=\begin{bmatrix} G_1(q_1,q_2) \\ G_2(q_1,q_2) \end{bmatrix},$$

$D_{11}(q_2)=m_1+m_2+2m_3\cos q_2,$

$D_{12}(q_2)=D_{21}(q_2)=m_2+m_3\cos q_2,$

$D_{22}(q_2)=m_2,$

$C_{11}(q_2)=-m_3\dot{q}_2\sin q_2,$

$C_{12}(q_1,q_2)=-m_3(\dot{q}_1+\dot{q}_2)\sin q_2,$

$C_{21}(q_1,q_2)=m_3\dot{q}_1\sin q_2,$

$C_{22}(q_2)=0,$

$G_1(q_1,q_2)=m_4 g\cos q_1+m_5 g\cos(q_1+q_2),$

$G_1(q_1,q_2)=m_5 g\cos(q_1+q_2)。$

Among them, $[m_1;m_2;m_3;m_4;m_5]=P+p_l L$, where P is the parameter vector of the robot itself, p_l is the load, $P=[1.66;0.42;0.63;3.75;1.25]$, $p_l=0.5$, $l_1=l_2=1.5$, and $L=\left[l_1^2;l_2^2;l_1l_2;l_1;l_2\right]$.

The Jacobian matrix parameters for the relationship between the speed of grinding the endpoint and the angular velocity of the robot joints are

$$J(q)=\begin{bmatrix} -l_1\sin(q_1)-l_2\sin(q_1+q_2) & -l_2\sin(q_1+q_2) \\ l_1\cos(q_1)+l_2\cos(q_1+q_2) & l_2\cos(q_1+q_2) \end{bmatrix},$$

$$\dot{J}(q)=\begin{bmatrix} -l_1\cos(q_1)-l_2\cos(q_1+q_2) & -l_2\cos(q_1+q_2) \\ -l_1\sin(q_1)-l_2\sin(q_1+q_2) & -l_2\sin(q_1+q_2) \end{bmatrix}\dot{q}_1+\begin{bmatrix} -l_2\cos\left(q_1+q_2\right) & -l_2\cos\left(q_1+q_2\right) \\ -l_2\sin\left(q_1+q_2\right) & -l_2\sin\left(q_1+q_2\right) \end{bmatrix}\dot{q}_2$$

The initial state of the robot end effector in Cartesian coordinates is $[0.85;1.1]$, then we take $\Delta=[\sin t;\cos t]$ and provide the expected end trajectory $l_{cx}=1-\cos(\pi t), l_{cy}=1+\sin(\pi t)$. We set the initial state of the robot impedance trajectory and the expected end position as $l_d(0)=l_c(0), \dot{l}_d(0)=\dot{l}_c(0)$. In addition, quality coefficient matrix $M=diag[1]$, damping coefficient matrix $B=diag[10]$, and stiffness coefficient matrix $K=diag[50]$.

To validate the effectiveness of the proposed integral sliding mode impedance method with the reaching law, a comparative simulation was conducted. The other two methods are the linear sliding mode impedance control method (LSMIC) and the integral sliding mode impedance method without integrating the exponential reaching law.

The design of the sliding surface for the linear sliding mode impedance control method is $s_1=\Lambda_1 e+\dot{e}$, and the control law is designed as follows:

$$F_{SMC} = D_l(\ddot{l}_d + \Lambda_1 \dot{e}) + C_l(\dot{l}_d + \Lambda_1 e) + G_l + F_{re} + Ks_1 + \eta \tanh \frac{s_1}{\varepsilon} \tag{14}$$

The sliding surface of the integral sliding mode impedance method without integrating the exponential reaching law is $s_2 = c_3 e + \dot{e} + c_4 \int e$, and the control law is designed as follows:

$$F_{l*} = D_l(\ddot{l}_d + c_3 \dot{e} + c_4 e) + C_l(\dot{l}_d + c_3 e + c_4 \int e) + G_l + F_{re} + Ks_2 + \eta \tanh \frac{s_2}{\varepsilon} \tag{15}$$

The control law of the integral sliding mode impedance method integrating the exponential reaching law adopts Equation (11). The parameters of the linear sliding mode controller are $\Lambda_1 = diag[10], K = diag[15], \eta = 1.2, \varepsilon = 0.5$. The parameters of the integral sliding mode controller without integrating the exponential reaching law are $c_3 = 60, c_4 = 60, K = diag[15], \eta = 1.2, \varepsilon = 0.5$. The parameters of the integral sliding mode controller integrating the exponential reaching law are $c_1 = 1000$, $c_2 = 1000$, $\varepsilon = 0.5$, $k = 10$.

To validate the efficacy of the impedance control method, obstacles were designed at position $l_x = 1$. When $l_x < 1$, the polishing robot is not in contact with the obstacle, and contact force $F_{re} = 0$, $l_d = l_c$. When $l_x > 1$, the polishing robot collides with an obstacle, and at this moment, $l \neq l_c, \dot{l} \neq \dot{l}_c, \ddot{l} \neq \ddot{l}_c, F_{re} \neq 0$, resulting in an impedance trajectory $l_d \neq l_c$.

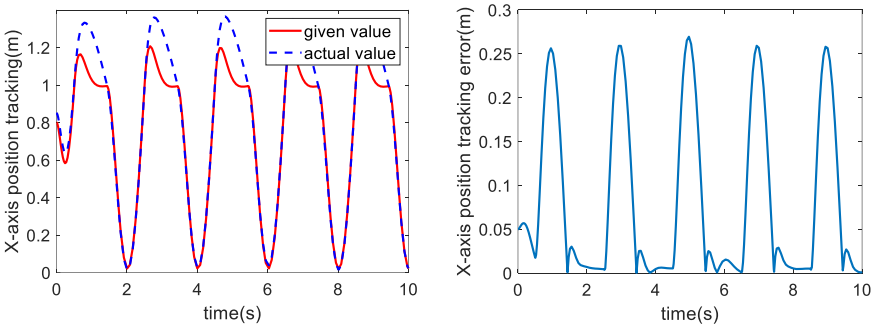

(a)X-axis position tracking (b)X-axis position tracking error

Fig. 1. X-axis position tracking under linear sliding mode method

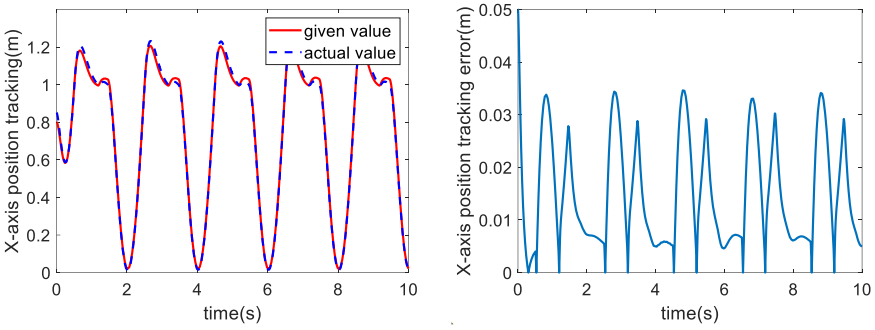

(a)X-axis position tracking (b)X-axis position tracking error

Fig. 2. X-axis position tracking under the integral sliding mode method without integrating the exponential reaching law

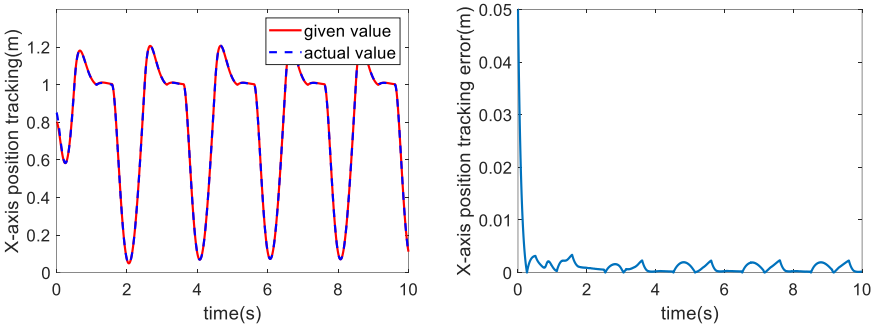

(a)X-axis position tracking (b)X-axis position tracking error

Fig. 3. X-axis position tracking under the integral sliding mode method integrating the exponential reaching law

Figures 1, 2, and 3 show the position tracking trajectories of actual end position trajectory l_x and ideal impedance position trajectory l_{dx} in the x-direction under the three methods and the position tracking error graphs of actual end position trajectory l_x in the x-direction and ideal impedance position trajectory l_{dx} under the three methods. The simulation results indicate that the maximum position tracking error in the x-direction can reach 0.25 m when employing the linear sliding mode method, which indicates suboptimal performance. When using the integral sliding mode method without integrating the exponential reaching law, the position tracking error in the x-direction can be controlled within 0.04 m, which is a significant improvement compared to the linear sliding mode method. When using the integral sliding mode method integrating the exponential reaching law, the position tracking error in the x-direction can be controlled within 0.005 m, and the effect is further improved.

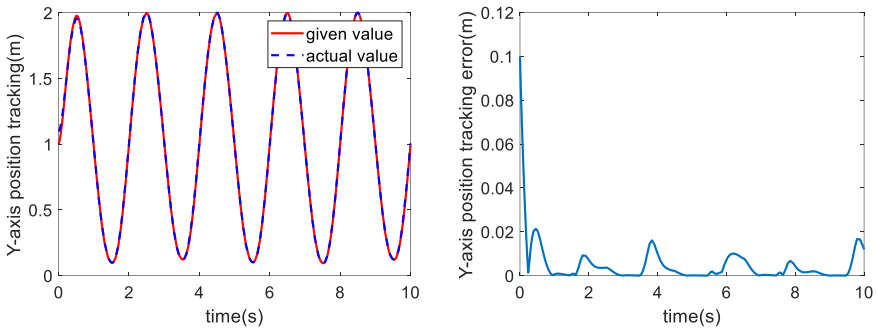

(a)Y-axis position tracking (b)Y-axis position tracking error

Fig. 4. Y-axis position tracking under linear sliding mode method

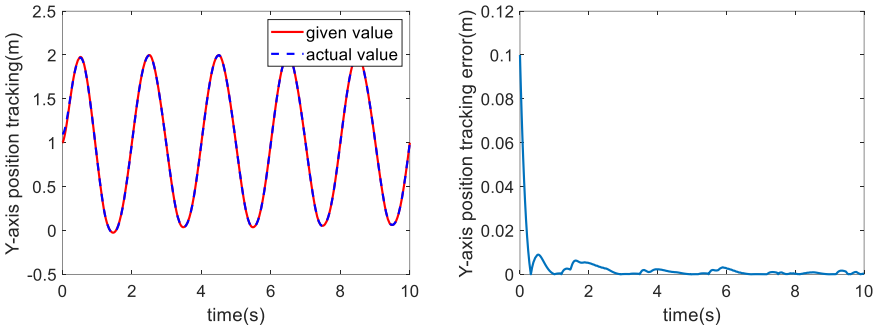

(a)Y-axis position tracking (b)Y-axis position tracking error

Fig. 5. Y-axis position tracking under the integral sliding mode method without integrating the exponential reaching law

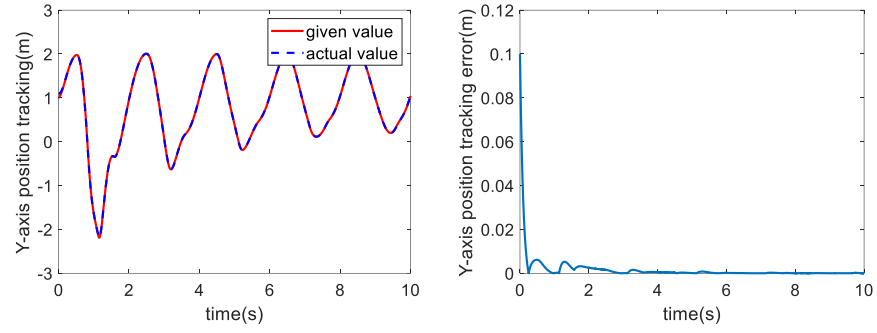

(a)Y-axis position tracking (b)Y-axis position tracking error

Fig. 6. Y-axis position tracking under the integral sliding mode method integrating the exponential reaching law

Figures 4, 5, and 6 show the position tracking trajectory diagrams of actual end position trajectory l_y and ideal impedance position trajectory l_{dy} in the y-direction under the three methods and the position tracking error graphs of actual end position trajectory l_y and ideal impedance position trajectory l_{dy} in the y-direction under the three methods. The simulation results demonstrate that all three control methods are capable of accurately tracking the desired impedance position trajectory in the y-direction. When using the linear sliding mode method, the position tracking error in the y-direction can be controlled within 0.025 m. The position tracking error in the y-direction can be controlled within 0.01 m using the integrated sliding mode method with or without integrating the exponential reaching law; the former has smaller error fluctuations after reaching stability compared to the latter.

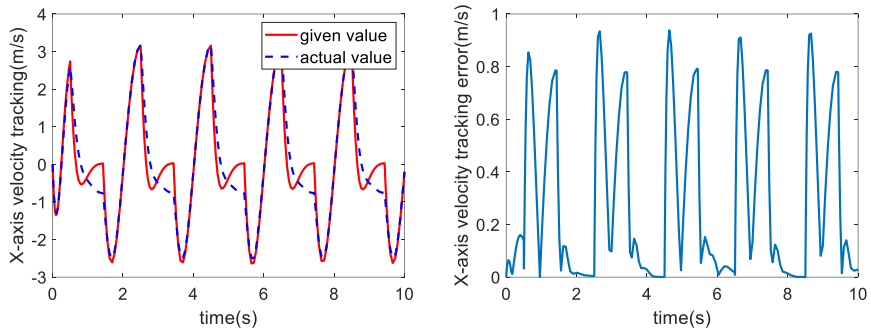

(a)X-axis velocity tracking (b)X-axis velocity tracking error

Fig. 7. X-axis velocity tracking under linear sliding mode method

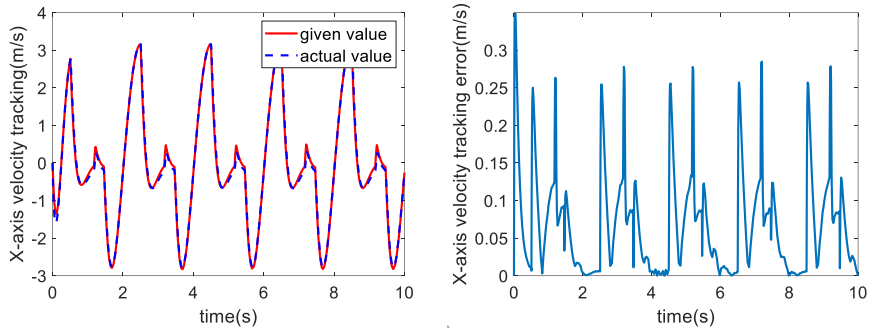

(a)X-axis velocity tracking (b)X-axis velocity tracking error

Fig. 8. X-axis velocity tracking under the integral sliding mode method without integrating the exponential reaching law

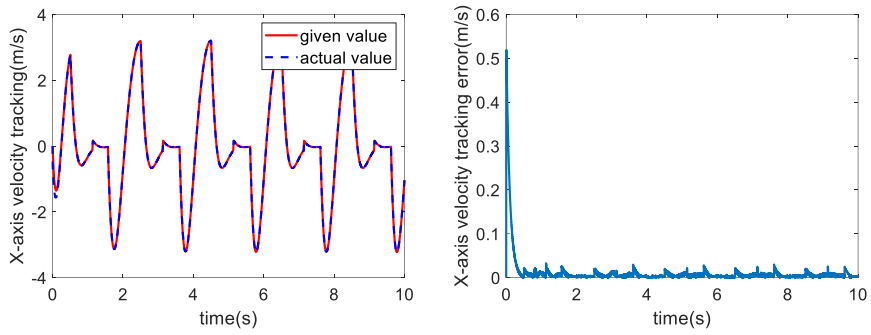

(a)X-axis velocity tracking (b)X-axis velocity tracking error

Fig. 9. X-axis velocity tracking under the integral sliding mode method integrating the exponential reaching law

Figures 7, 8, and 9 show the velocity tracking trajectories of the actual end velocity trajectory $\dot{l}_x$ and the ideal impedance velocity trajectory $\dot{l}_{dx}$ in the x-direction under the three methods and the position tracking error graphs of the actual end velocity trajectory $\dot{l}_x$ in the x-direction and the ideal impedance velocity trajectory $\dot{l}_{dx}$ under the three methods. The simulation results indicate that the maximum velocity tracking error in the x-direction can reach approximately 0.9 m/s when using the linear sliding mode method, which is not ideal. When using the integral sliding mode method without integrating the exponential reaching law, the velocity tracking error in the x-direction can be controlled within 0.3 m/s, which is a significant improvement compared to the linear sliding mode method. When using the integral sliding mode method integrating the exponential reaching law, the velocity tracking error in the x-direction can be controlled within 0.05 m/s, further improving the effect. What's more, in the y-direction, the velocity trajectories controlled by the three methods have also achieved similar results.

5 Experimental validation

In this section, experimental validation and analysis are carried out to further confirm the effectiveness of the proposed impedance control method. Figure 10 presents the grinding robot experimental system, which includes a Sawyer robot, a torque sensor, a high-speed electric spindle, a grinding tip, and a cylinder block.

A comparative experiment is performed using the LSMIC and the ERL-ISMIC. Under the action of the controller, all joints can achieve stable operation, as shown in Figure 11, which illustrates the movement of four of these joints. Specifically, under the influence of LSMIC, the maximum steady-state errors of the four joints are 1.98, 3.75, 0.83, and 4.84, respectively. In contrast, under the effect of ERL-ISMIC, the maximum steady-state errors of the four joints are 0.49, 1.48, 0.25, and 0.85, respectively. Therefore, the ERL-ISMIC designed in this paper improves the steady-state performance of the grinding robot control system.

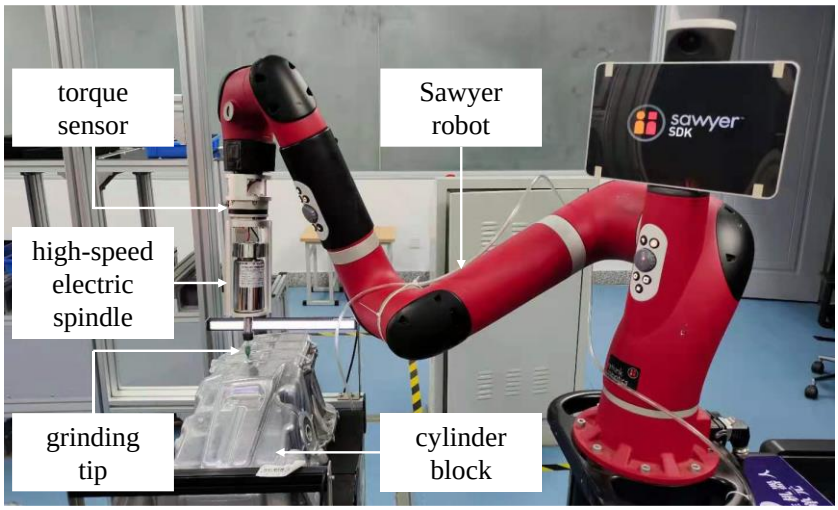

Fig. 10. Grinding robot experimental system

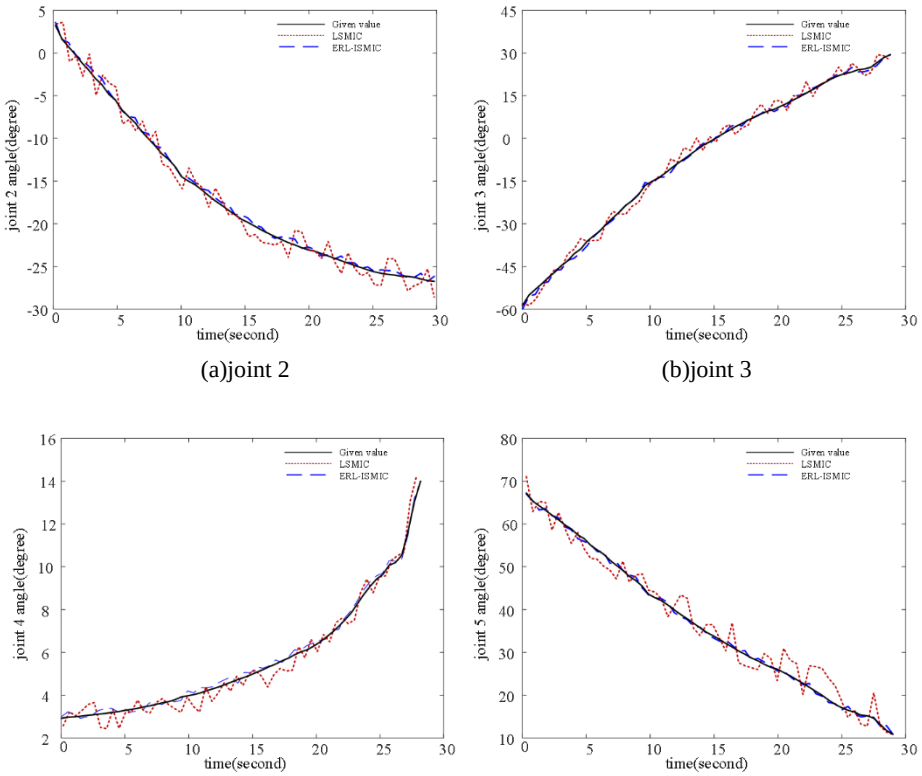

(a)joint 2 (b)joint 3

(c)joint 4 (d)joint 5

Fig. 11. Joint position tracking of grinding robot

6 Conclusion

To tackle the challenge of achieving high-precision grinding on free-form surfaces, an integral sliding mode impedance control method for grinding robots is proposed, utilizing the exponential reaching law. Firstly, the contact force between the robot and the workpiece is determined based on the impedance model and the tracking error. Subsequently, the ideal trajectory in Cartesian space is converted into an impedance trajectory, guided by this contact force. Then, an integral sliding mode impedance control method is developed to track the modified impedance trajectory, significantly mitigating the chattering phenomenon inherent in sliding mode control, thanks to the utilization of the exponential reaching law. Finally, the control system's stability is verified through the application of Lyapunov stability theory, and recommendations for parameter selection are provided. Simulation and experimental results reveal that, compared to linear sliding mode and conventional integral sliding mode methods, the method presented in this paper exhibits superior dynamic and static performance.

Acknowledgments. This work was supported by the National Natural Science Foundation of China 62303178, 62173137, 62073131, the Hunan Provincial Natural Science Foundation of China 2024JJ7139, the Project of Hunan Provincial Department of Education 23A0426 and the Science and Technology Innovation Program of Hunan Province 2021RC3122.

References

1. Gracia L, Solanes J E, Munoz-Benavent P, et al.: Adaptive sliding mode control for robotic surface treatment using force feedback[J]. Mechatronics 52, 102-118(2018).
2. Huo Y, Li P, Chen D, et al.: Model-free adaptive impedance control for autonomous robotic sanding[J]. IEEE Transactions on Automation Science and Engineering 19(4), 3601-3611(2021).
3. Han F T, Tam S Y, Cao Z H, et al.: Nonlinear impedance control with trajectory adaptation for collaborative robotic grinding[J]. Science China Technological Sciences 66(7), 1928-1936(2023).
4. Wang G, Deng Y, Zhou H, et al.: PD-adaptive variable impedance constant force control of macro-mini robot for compliant grinding and polishing[J]. The International Journal of Advanced Manufacturing Technology 124(7), 2149-2170(2023).
5. Wang T, Sun Z, Song A, et al.: Sliding mode impedance control for dual hand master single slave teleoperation systems[J]. IEEE Transactions on Intelligent Transportation Systems 23(12), 25500-25508(2021).
6. Dai P, Lu W, Le K, et al.: Sliding Mode Impedance Control for contact intervention of an I-AUV: Simulation and experimental validation[J]. Ocean Engineering 196, 106855(2020).
7. Rong Y, Chou W, Jiao R.: Robust fault-tolerant motion/force control of a fully-actuated hexarotor using adaptive sliding mode impedance control[J]. International Journal of Robust and Nonlinear Control 32(7), 4149-4172(2022).
8. Zheng G, Lei J, Hu L, et al.: Fuzzy adaptive sliding mode impedance control of fracture reduction robot[J]. IEEE Access 9, 113653-113665(2021).

9. Wu Q, Xu D, Chen B, et al.: Integral fuzzy sliding mode impedance control of an upper extremity rehabilitation robot using time delay estimation[J]. IEEE Access 7, 156513-156525(2019).
10. Adamiak K, Bartoszewicz A.: Novel power-rate reaching law for quasi-sliding mode control[J]. Energies 15(15), 5446(2022).
11. Haroon F, Aamir M, Waqar A. : Second-order rotating sliding mode control with composite reaching law for two level single phase voltage source inverters[J]. IEEE Access 10, 60177-60188(2022).
12. He J, Tang R, Wu Q, et al.: Robust predictive current control of permanent magnet synchronous motor using voltage coefficient matrix update[J]. International Journal of Electrical Power & Energy Systems 159, 109999(2024).
13. Prasun P, Kamal S, Bartoszewicz A, et al.: Difference equation with minima-based discrete-time sliding mode control[J]. IEEE Transactions on Circuits and Systems II: Express Briefs 70(12), 4404-4408(2023).
14. Qu Y, Zhang B, Chu H, et al.: Sliding-mode anti-disturbance speed control of permanent magnet synchronous motor based on an advanced reaching law[J]. ISA transactions 139, 436-447(2023).
15. Feng L, Sun X, Guo D, et al.: Advanced torque sharing function strategy with sliding mode control for switched reluctance motors[J]. IEEE Transactions on Transportation Electrification 10(1), 2302-2311(2023).
16. Spyrakos-Papastavridis E, Childs P R N, Dai J S.: Passivity preservation for variable impedance control of compliant robots[J]. IEEE/ASME Transactions on Mechatronics 25(5), 2342-2353(2019).
17. Peng G, Chen C L P, Yang C.: Robust admittance control of optimized robot–environment interaction using reference adaptation[J]. IEEE Transactions on Neural Networks and Learning Systems 34(9), 5804-5815(2022).
18. Zhou K, Wang S, Zhou R, et al.: Admittance control design and system testing of industrial robot polishing operation[J]. Proceedings of the Institution of Mechanical Engineers, Part B: Journal of Engineering Manufacture 237(10), 1538-1552(2023).
19. He G, Fan Y, Su T, et al.: Variable impedance control of cable actuated continuum manipulators[J]. International Journal of Control, Automation and Systems 18(7), 1839-1852(2020).
20. Stolfi A, Gasbarri P, Sabatini M.: A combined impedance-PD approach for controlling a dual-arm space manipulator in the capture of a non-cooperative target[J]. Acta Astronautica 139, 243-253(2017).
21. Li Y, Wang D.: Servo motor sliding mode control based on fuzzy power index method[J]. Computers & Electrical Engineering 94, 107351(2021).
22. Miao X, Yao W, Ouyang H, et al.: Novel Composite Speed Control of Permanent Magnet Synchronous Motor Using Integral Sliding Mode Approach[J]. Mathematics 11(22), 4666(2023).
23. Iyer A G, Samantaray J, Ghosh S, et al.: Sliding mode control using power rate exponential reaching law for urban platooning[J]. IFAC-PapersOnLine 55(1), 516-521(2022).
24. Zhai J, Xu G.:A novel non-singular terminal sliding mode trajectory tracking control for robotic manipulators[J].IEEE Transactions on Circuits and Systems II: Express Briefs 68(1)，391-395(2020).
25. Cui S, Song H, Zheng T, et al.: Trajectory Tracking Control of Mobile Manipulator Based on Improved Sliding Mode Control Algorithm[J]. Processes 12(5), 881(2024).